Vela pulsar observations with the Ooty Radio Telescope

Kishalay De
Indian Institute of Science

1 Introduction

We have been given a sample of the voltage signal obtained from an observation of the Vela pulsar (PSR B0833-45) with the Ooty Radio Telescope. The Ooty Radio Telescope consists of a cylindrical paraboloid reflecting surface which is 530 m long and 30 m wide, placed on a slope of 11.2 degrees in the north-south direction in Muthorai village near Ooty. The signal detectors consist of an array of 1056 half-wave dipoles which are operated to produce phased array beams in the sky.

Over the course of this analysis, we will try to investigate some of the statistical, time-domain and frequency-domain properties of the signal, and extract some information about the observed pulsar. The observation has been conducted at 326.5 MHz with a bandwidth of 16.5 MHz, and the voltage signals from the northern and southern half of the telescope is available to us. Note that we will not use any specific set of units to quantify the voltage or the intensity signals, since no calibration data has been provided.

2 Signal statistics

2.1 Voltage signal characteristics

We would first like to investigate the statistical properties of the voltage signal received at the telescope to verify some of its expected properties. We expect the voltage signal to have a Gaussian distribution with some mean and standard deviation. Let us have a look at the histograms of the voltage received at the northern and southern feeds of the telescope. To ensure that the presence of the pulsar signal within this time series (where one would expect increased levels of power) does not affect the general statistical conclusions, we start with a set of 100,000 voltage samples which have been randomly and uniformly selected from the data set (a thousandth fraction of the entire sample).

While it is evident that the distributions have a characteristic Gaussian shape, we will verify this further. We estimate the mean and variance of the two voltage samples using the unbiased estimators for the parameters. For the northern half voltage, these parameters are:

$$\mu_{North} = 3.445 \quad \sigma_{North} = 28.142 \tag{1}$$

The same set of parameters for the voltage obtained from the southern half is:

$$\mu_{South} = 0.610 \quad \sigma_{South} = 29.838 \tag{2}$$

With these parameter estimates, we scale the entire data set to a normalized distribution using,

$$X_{new} = \frac{X_{old} - \mu}{\sigma} \tag{3}$$

where X_{new} is the scaled voltage, X_{old} is the original randomly sampled voltage, μ is the distribution mean and σ is the standard deviation for the northern and southern

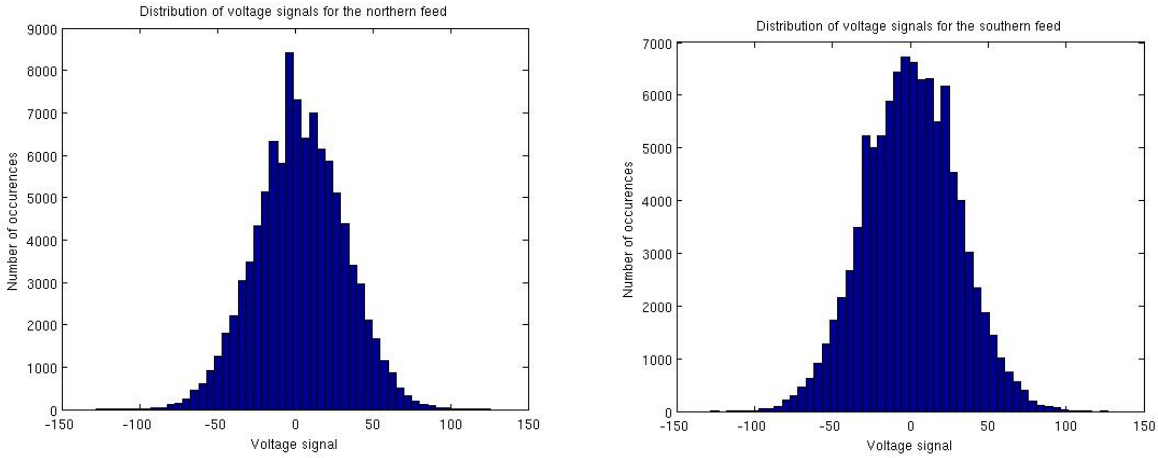

(a) Histogram of the voltage at the northern half (b) Histogram of the voltage at the southern half

Figure 1: Histograms for the voltage distributions for a total of 100,000 randomly selected samples

half voltages respectively. We now test the hypothesis that these distributions follow a standard normal distribution with the Student's t-test, which gives a p-value of $\sim 10^{-14}$ less than 1 in favor of the null hypothesis, for both the northern and southern feed voltages. Clearly, it can be concluded with a high level of confidence that these voltages follow a normal distribution.

We can now proceed to estimate the statistical parameters and their confidence intervals for the voltage signals. We then get,

$$\mu_{North} = 3.445 \pm 0.174 \quad \sigma_{North} = 28.142 \pm 0.124$$
$$\mu_{South} = 0.610 \pm 0.185 \quad \sigma_{South} = 29.838 \pm 0.131$$

where the intervals correspond to 95% confidence bounds. Note that the voltage values do not have a zero mean as one would have expected. This may result from small bias voltages in the telescope back-end, which would add an offset to all voltages.

2.2 Power signal characteristics

We now investigate the properties of the intensity signal, i.e., the square of the voltage signal. We expect the signal to have an exponential distribution with equal mean and standard deviation. The histogram of the power signals of the northern and southern feeds are given in Figure 2 (for the same set of samples). The distributions are well fit with an exponential curve. We now estimate the mean and standard deviation of this distribution. Note that

$$E[X] = \sum p_i X_i \tag{4}$$

where p_i is the probability (obtained from the histogram by dividing the number of counts in a bin by the total number of counts) and X_i is the value of the variable. Again,

$$Var[X] = E[X^2] - E[X]^2 \tag{5}$$

Using these relations, we get $E[X] = 832.43$ and $Var[X] = 122.71 \times 10^4$, which gives $\sigma[X] = \sqrt{Var[X]} = 1107.75$. Though $\sigma[X]$ and $E[X]$ have values which are fairly close

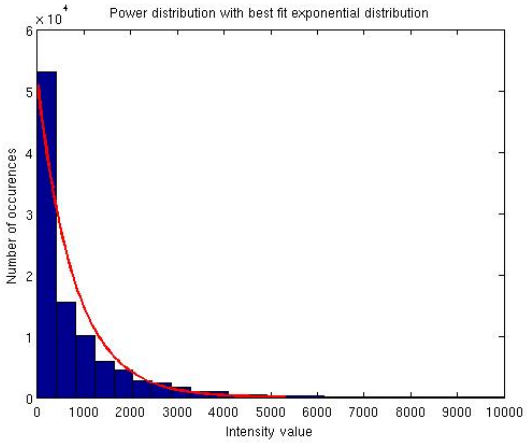

(a) Intensity signal distribution for the northern half.

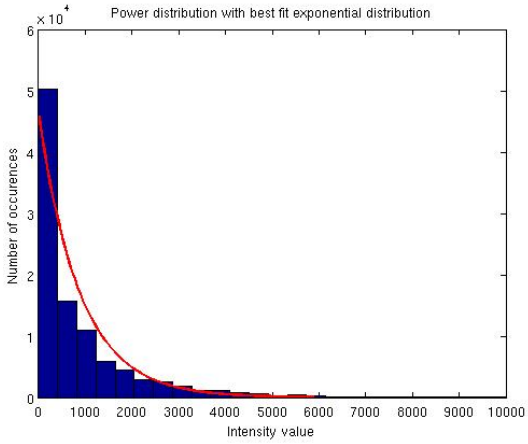

(b) Intensity signal distribution for the southern half.

Figure 2: Distributions of the intensity signal for the two halves of the telescope, along with best-fit exponential distributions.

as expected, they are not equal. This may be an effect of the quantization of a continuous distribution by binning into a histogram and from the earlier observed offset from zero mean in the voltage distributions, which would create deviations from a pure exponential distribution.

3 Time-Frequency domain properties

3.1 The voltage power spectrum

We would now like to analyze the signal in the frequency domain. It has been told that the observations have been carried out with a bandwidth of 16.5 MHz. Consequently, it would be interesting to see the power spectrum of the voltage signal to identify any signs of aliasing in the frequency domain. Using the Fast Fourier Transform (FFT) with 256 frequency channels (a sufficient frequency resolution of $\sim$ 125 kHz; power of 2 increases the speed of the FFT), we find the average power spectrum of the voltage signal by averaging the power spectrum obtained from all 512-point (time samples) FFTs. The spectra for the northern and southern half are given below.

A number of interesting points can be observed from these spectra. Firstly, note that the 0 frequency channels has a large signal (much larger than its nearby channels), indicating that there is a DC offset in the voltage time series. This reinforces the claim made at the end of Section 2.1 to explain the non-zero mean in the voltage. Secondly, it is easy to see that the DC channel power is much larger in the northern signal, than the southern signal which is consistent with the fact that the norther signal voltage mean is much larger than the southern signal mean, which is closer to zero. Finally, we can clearly see that the power spectrum smoothly tapers off to zero at both the edges of the band, indicating that aliasing is very minimal for these receivers. The sharp peaks in the spectra may be signatures of local Radio Frequency Interference (RFI).

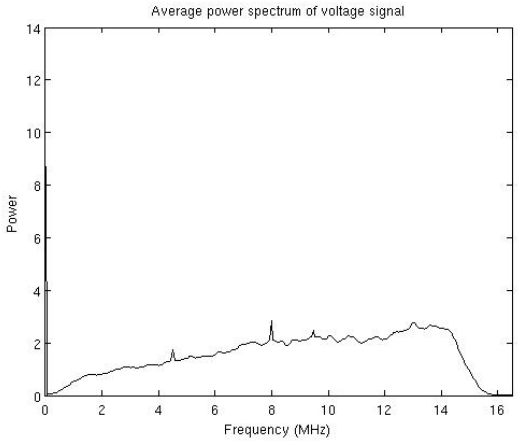

(a) Power spectrum from the northern half

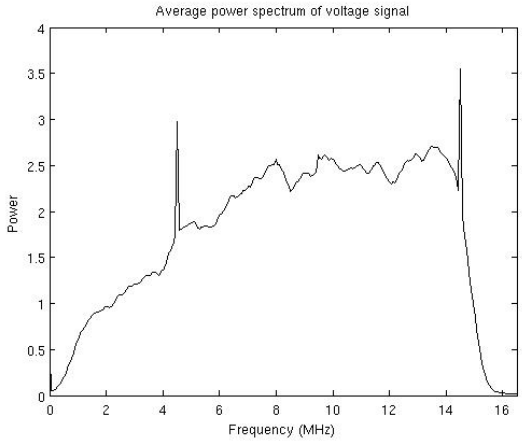

(b) Power spectrum from the southern half

Figure 3: Average power spectrum from the two feeds in the telescope. The frequency axis goes from 0 to 16.5 MHz, corresponding to the bandwidth of the receiver.

3.2 Dynamic spectrum

We now try to detect the first signs of the pulsar signal by looking at the dynamic spectrum of the signal, i.e., the power in the signal as a function of time and frequency. As a trial, we examine ∼350 ms of the data to detect a pulsed signal, if present. The dynamic spectrum is shown below, where the y-axis is frequency in MHz, x-axis is time in ms and the color code indicates the signal power for a particular frequency and time sample. To improve the Signal to Noise Ratio (SNR) of the signal, the power from the two halves of the array have been added (Incoherent addition). Note that the maximum time delay between the northern and the southern half of the array is of the order of 500 m / c $\sim$ 1 μs, which is much smaller than the time resolution we have used and hence delay correction will not affect our analysis.

Clearly, there is an interesting source visible in the plot. A pulsed signal appears earliest at the high frequencies, and gradually appears later at lower frequencies. Four such pulses are visible in the dynamic spectrum. This frequency dependent delay is a characteristic sign of a signal dispersed in the interstellar medium. The observed delays can be used to estimate the Dispersion Measure (DM) along the line of sight to the pulsar.

4 Discovering the pulsar

4.1 Pulse time of arrival and the Dispersion Measure

Given the limited amount of data, estimating pulse time arrivals as a function of frequency is a fairly difficult task because of a couple of reasons:

- Single pulses in individual frequency channels have very low SNR to allow a useful calculation. Hence, we need to increase the bandwidth of individual channels to get better SNR.
- We cannot increase the channel-width as much as we would like to, since remaining dispersion within the channels would spoil the signal.

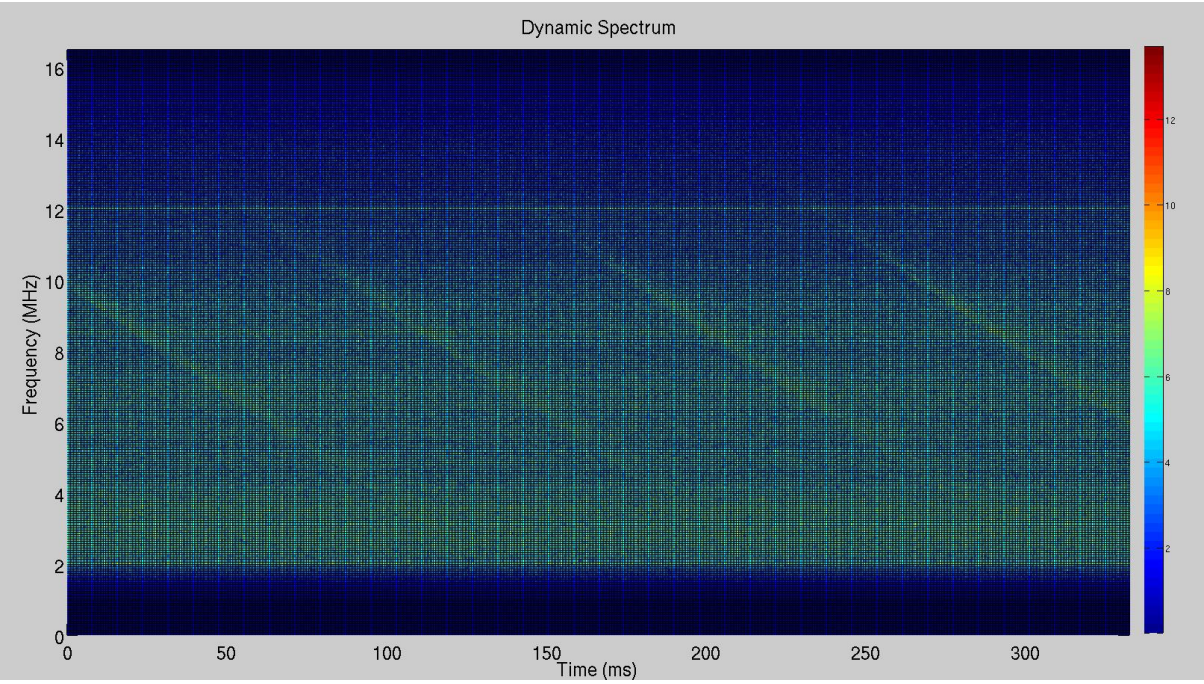

Figure 4: The dynamic spectrum of the signal for the first $\sim$ 350 ms. Frequency is plotted on the y-axis, and increases upwards from the lower edge of the band to the upper edge. Frequency resolution is 125 kHz. Time is plotted on the x-axis for a duration of 200 ms, and a time resolution of $\sim$ 490 μs. The power from the northern and southern half of the telescope have been added to increase the SNR.

Hence, we now use 64 channels (corresponding to channel width of 500 kHz) across the band to increase the SNR of single pulses. Given that we do not know the period of the pulsar, we cannot fold the profile to obtain better SNR either. Hence, we use one strong pulse in the data set to estimate the time at which it arrives at three different frequencies, and subsequently obtain the Dispersion Measure along the given direction. Note that we are limited to using the frequency channels which have the strongest signals (verified visually), ans other frequency channels have significantly poorer SNR for single pulses.

To obtain the time of arrival of the pulse in different frequency channels, we fit the single pulse to a Gaussian curve, and use the mean of the Gaussian to estimate the arrival time with respect to the start of the voltage stream. The fit Gaussians and the relevant parameters are given in Figure 4. It should be noted that the pulse arrival times are essentially arrival times for the pulse across a 500 kHz bandwidth, and by approximating this channel by its center frequency, we may overestimate the DM. Furthermore, we are assuming that the pulse shapes are well-fit with a Gaussian curve. While this is true for a lot of pulsars, it may not be completely accurate in this case.

Now, the pulse arrival time at a frequency ν (in MHz) depends on the DM (in pc/cc) of the pulsar as (see NRAO website in References),

$$t \approx t_\infty + 4.149 \times 10^3 \times DM \times \nu^{-2} \tag{6}$$

where t is the pulse arrival time in seconds and t_∞ is the pulse arrival time in seconds at infinite frequency. Clearly, a plot of t vs. ν^{-2} would provide us with the information

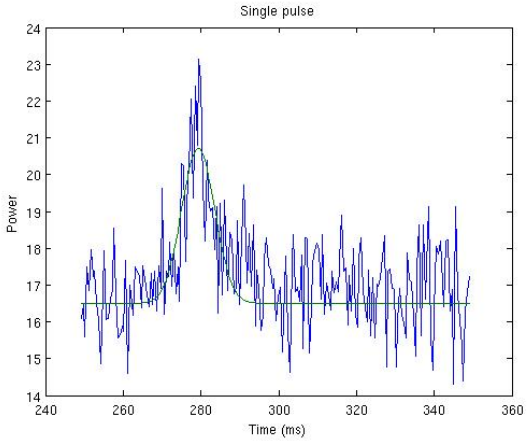

(a) Single pulse and best fit Gaussian at 327.918 MHz across 500 kHz channel width. Pulse arrival time estimated to be 279.3 ± 0.8 ms.

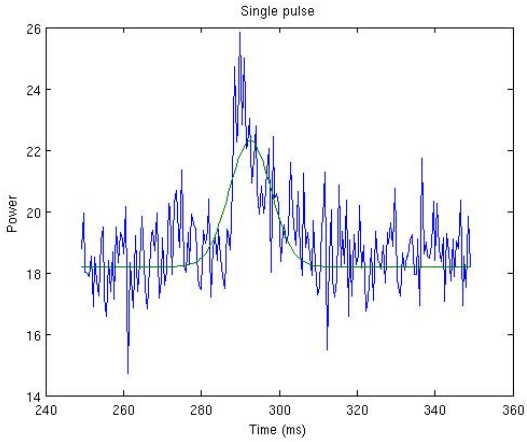

(b) Single pulse and best fit Gaussian at 327.209 MHz across 500 kHz channel width. Pulse arrival time estimated to be 292.6 ± 1.1 ms.

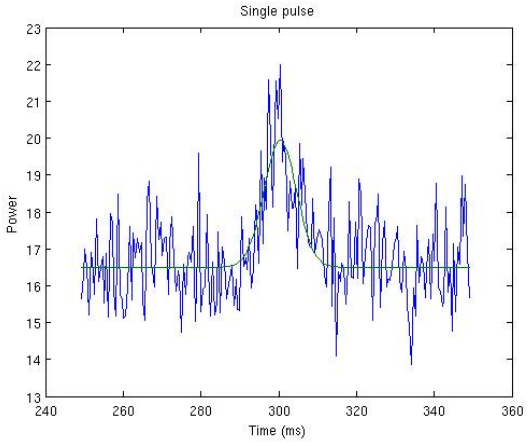

(c) Single pulse and best fit Gaussian at 326.500 MHz across 500 kHz channel width. Pulse arrival time estimated to be 300.4 ± 1.0 ms.

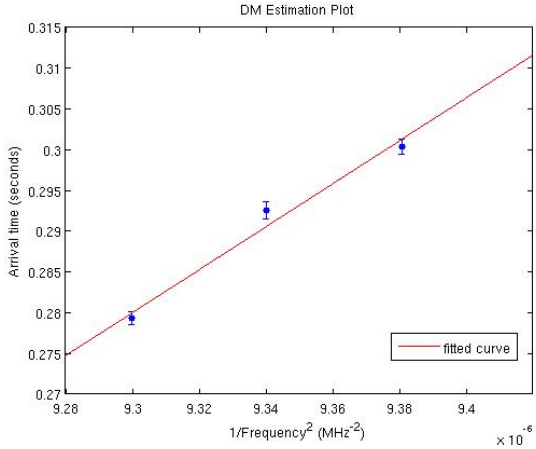

(d) Plot of arrival time (s) with respect to start of observation vs. ν^-2 (in MHz$^-2$). Measured slope is $(2.636 \pm 0.635) \times 10^5$ s MHz^{-2}.

Figure 5: Estimation of pulse arrival times across the band and the DM along the line of sight to the pulsar. Time resolution used is $\sim$ 490 μs.

required to calculate the DM. From the information given in, we plot time of arrival as a function of ν^{-2} and fit it with a straight line, as shown in Figure 4. The slope of the line is $(2.636 \pm 0.635) \times 10^5$ s MHz^{-2} where the uncertainty is at the 68 % confidence interval. Hence, the DM estimate for the pulsar is 63.5 ± 15.3 pc/cc based on Equation 6.

Assuming the mean electron density in the galactic medium to be $n_e = 0.03$ cc^{-1}, we estimate a distance of 2.11 ± 0.51 kpc to the pulsar.

4.2 Dedispersion

We can now dedisperse this signal by correcting for the frequency dependent delays using our knowledge of the DM. Going back to our original 256 channel resolution (to minimize intra-channel smearing), and following Equation 6, we correct for the frequency dependent term by applying the required time delays to the frequency channels. From Equation 6,

it immediately follows that the delay between two frequency channels at ν_1 and ν_2 MHz will be,

$$\tau(s) = 4.149 \times 10^3 \times DM \times (\nu_1^{-2} - \nu_2^{-2}) \quad (7)$$

We adjust the time-domain position of all lower frequency channels to align them with the pulse arrival time at the highest channel and then add the intensity in all the channels to obtain the dedispersed signal intensity. The result of the procedure is shown in Figure 6.

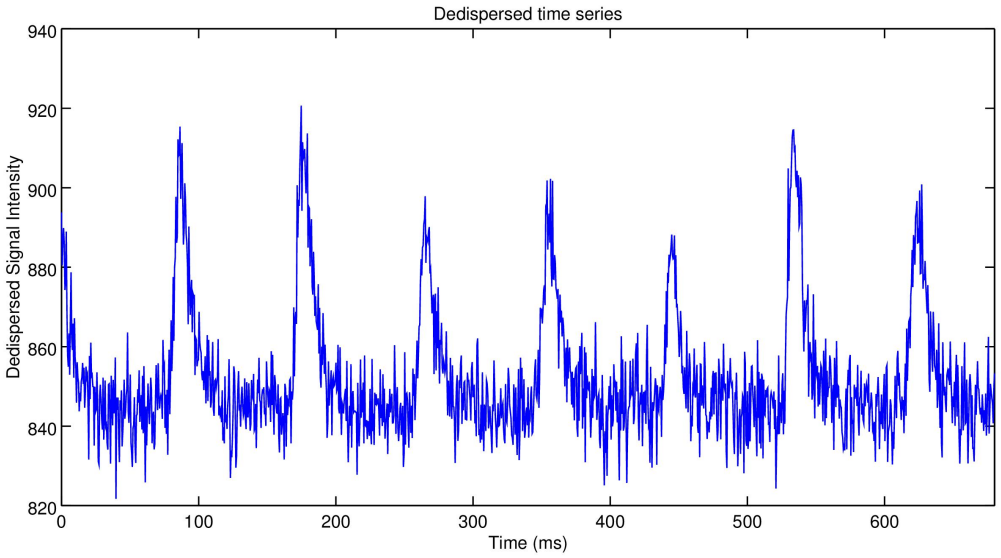

Figure 6: The dedispersed time series of the voltage stream provided with 256 frequency channels. The DM used is 63.5 pc/cc (as obtained earlier) and time resolution used is $\sim$ 490 μs.

It is evident that the single pulses now have significantly higher SNR, and are clearly visible above the background noise. Note that the length of the time series has been shortened because time delays could not be applied to channels where the pulse did not arrive at the lower edge of the band before the end of the observation.

4.3 The pulsar period

With a number of high SNR single pulses available, we are now in a position to estimate the periodicity of the signal, i.e., the rotation period of the pulsar. We require the arrival times of the individual pulses to fit a period solution, and hence, we go back to an earlier technique of fitting Gaussian curves to individual pulses, to estimate the arrival times. An example of a fit pulse is shown in Figure 7 (a). The obtained arrival times for each of the pulses with the respect to the start of the observation (starting from the second visible pulse in Figure 6), along with their uncertainties are given in Table 1. A linear fit to the arrival times is shown in Figure 7 (b).

The best-fit linear parameters for the given fit is P = 89.46 ± 0.14 ms, where P is the pulsar period. Note that a second order polynomial fit yields a $\dot{P}$ which is consistent with 0, and hence $\dot{P}$ cannot be estimated with such a short length of data. Finally, based on the period estimated, we can fold the entire time series with the pulsar period to obtain an average profile for the pulsar. This is shown in Figure 8. Note that the average profile indicates that our initial assumption for a Gaussian pulse shape is fairly accurate.

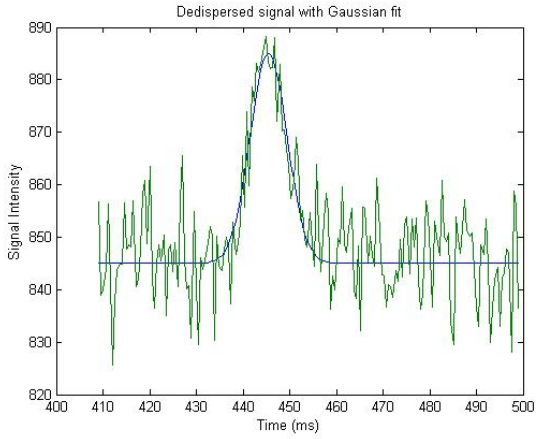

(a) A dedispersed single pulse with a Gaussian fit.

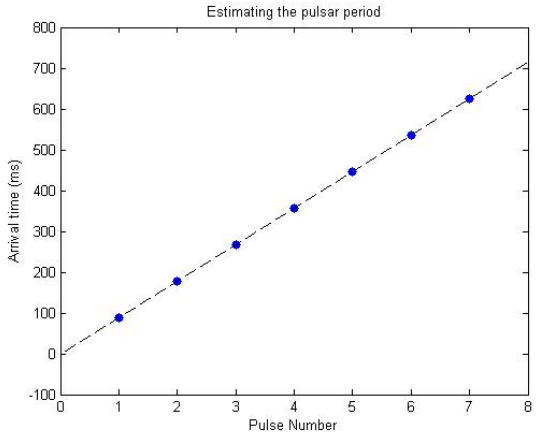

(b) A linear fit to the pulse arrival times to estimate the rotation period.

Figure 7: Estimating the pulsar period by fitting single pulses with Gaussian curves, followed by fitting the estimated arrival times with a linear curve.

Pulse Number	Arrival time (ms)	Uncertainty (ms)
1	88.09	0.50
2	177.50	0.45
3	266.80	0.55
4	356.80	0.66
5	445.50	0.55
6	535.10	0.50
7	625.20	0.60

Table 1: Pulse arrival times for the given data set

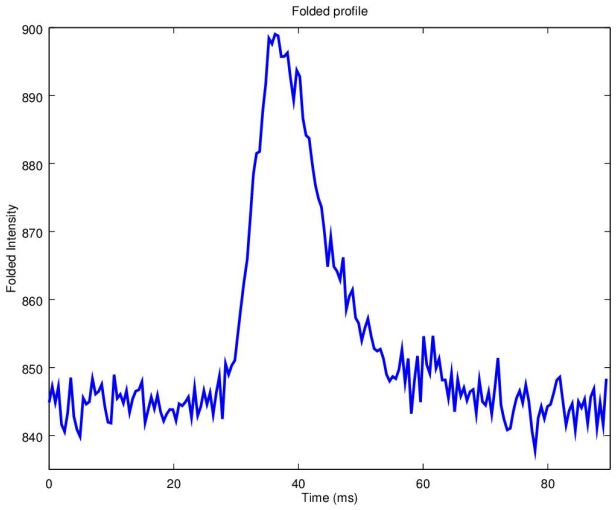

Figure 8: The average profile of the pulsar, folded with the estimated pulsar period.

5 Conclusions

After this long effort, we have managed to investigate a number of interesting characteristics of the signal. Starting from a statistical examination of the properties of the voltage signal to estimating the DM of the pulsar, up to estimating the period of the pulsar, we have recovered a number of useful parameters with this rather small data set, albeit with a fair amount of uncertainty. Note that all quantitative estimates, including that of the pulsar period may be corrupted by the large uncertainties in other parameters, especially the DM. Indeed, longer observations would help to significantly reduce these error bars, and possibly better knowledge of the observing time and configuration would allow one to phase the two halves of the array to increase sensitivity.

The visibilities of the source from the two arrays have not been calculated, primarily because interferometry cannot be done using the limited information available. More specifically, the observing time, and the exact location of the phase centers for these two halves would be required to calculate the projected baselines with respect to the source. However, we can expect that the visibilities would remain constant as a function of time, because the source is a compact object, i.e., the equivalent of a delta function in the sky. Hence, the Fourier transform of this brightness distribution would be a constant across all baselines, and therefore, will not change even as the projected baseline changes with time.

6 References

- Pulsars. Website of the National Radio Astronomy Observatory. Available at www.cv.nrao.edu/course/astr534/Pulsars.html. Accessed 15 Nov, 2015.
- J. N. Chengalur, Y. Gupta & K. S. Dwarkanath, Low Frequency Radio Astronomy, 2003.
- D. R. Lorimer & M. Kramer, Handbook of Pulsar Astronomy, Vol.4, Cambridge University Press (2004).